

Stable reconstruction of the polar (111) surface of NiO on Au(111)

C. A. Ventrice, Jr.,* Th. Bertrams, H. Hannemann, A. Brodde,[†] and H. Neddermeyer
Institut für Experimentalphysik, Ruhr-Universität Bochum, Postfach 102148, D-44780 Bochum, Germany
 (Received 29 October 1993)

Several theoretical studies of the stability of (111)-terminated ionic crystals with the NaCl structure have predicted that the crystal Madelung energy can be stabilized by a simple surface reconstruction. However, previous attempts to grow (111)-terminated crystals have resulted in either unreconstructed or faceted surfaces. We demonstrate that deposition of Ni in an oxygen atmosphere onto a Au(111) substrate held at $T \sim 300^\circ\text{C}$ results in the growth of a stable $p(2 \times 2)$ reconstructed NiO(111) and resolve the atomic details of this surface with our scanning tunneling microscope.

The stability of ionic materials with polar surface terminations has been given considerable attention for several years.¹⁻⁵ Due to the long-range $1/r$ term in the Coulomb potential, one finds that the electrostatic energy of an ionic crystal is conditionally convergent. One technique which is used to overcome this problem is to perform a shellwise summation of units within the crystal which have vanishing monopole and dipole moments. For crystals with the NaCl structure, a summation technique based on the octopole approximation, which was originally proposed by Lacmann,¹ is often used. This technique models the NaCl crystal as a simple-cubic lattice with a $(\text{NaCl})_4$ basis instead of the conventional face-centered-cubic (fcc) lattice with a dipolar NaCl basis. The lowest-order moment of the $(\text{NaCl})_4$ basis cubes is octopolar, and thus the interaction between them falls off as $1/r^7$. Most recently, a study by Wolf⁵ which includes relaxation effects has predicted that the polar (111) surface of crystals with the NaCl structure which have the octopolar termination should be stable at zero temperature. The polar (111) surface of a NaCl crystal constructed from a $(\text{NaCl})_4$ basis is shown in Fig. 1.

For covalently bonded crystals with a partial ionic character, there are many examples of polar surfaces which undergo simple reconstructions.² However, for highly ionic crystals which exhibit the NaCl structure, we know of no known study where one was able to grow a crystal with a stable reconstructed polar surface except by the creation of large-scale facets. There are some instances, though, where unreconstructed polar surfaces of crystals with the NaCl structure have been reported. In the case of NiO(111), this stability was achieved by the addition of some form of surface contaminant such as by Si (Ref. 6) or Pb (Ref. 7) segregation or by OH adsorption.⁸ For the case of the MgO(111) surface, it has been theorized that its stability results from a change in the charge state of the surface atoms.³ Unfortunately, this charge transfer mechanism has not been substantiated by experiment.

Most metal oxides are wide band-gap insulators (for bulk NiO, $E_{\text{gap}} = 4.0$ eV) (Ref. 9) which can result in sample charging problems when performing spectroscopic techniques involving charged particles. Therefore, there have been relatively few studies of the electronic properties and geometric structure of metal oxide sur-

faces¹⁰ when compared to the degree of work performed on metal and semiconducting surfaces. One technique which has been used to try to overcome this problem is oxidation of the surface region of a single-crystal metal substrate. It has been shown that this procedure can result in an ordered oxide which is thick enough to exhibit the physical properties of a bulk single crystal yet thin enough to allow tunneling of excess charge into the metal substrate.¹¹ Since there is, in general, a very large lattice mismatch between a metal crystal and its corresponding oxide, the metal oxide films grown in this manner often have a very large defect density.¹² In order to circumvent the lattice mismatch problem, the growth of an ordered NiO(111) film by deposition of Ni in an oxygen atmosphere onto a Au(111) surface has been attempted since the lattice mismatch of NiO and Au is only $\sim 2\%$ ($a_{\text{Au}} = 4.08$ Å, $a_{\text{NiO}} = 4.17$ Å). For NiO growth on a Au(111) crystal held at room temperature, we have found that a three-domain NiO(100) overlayer is primarily formed. However, for growth on a Au(111) crystal at $T \sim 300^\circ\text{C}$, the formation of $p(2 \times 2)$ reconstructed NiO(111) is preferred. To the best of our knowledge, this is the first reported observation of a simply reconstructed (111) surface for an ionic NaCl structured material. Although a recent publication by Weiss and Somorjai¹³ has also indicated that a stable $p(2 \times 2)$ reconstructed FeO(111) overlayer can be grown on Pt(111), subsequent structural low-energy electron diffraction (LEED) analyses¹⁴ of this surface indicate that an unreconstructed $\text{Fe}_3\text{O}_4(111)$ surface was actually formed.

These experiments were conducted in an ultrahigh vac-

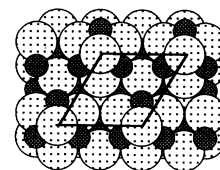


FIG. 1. Schematic of the top view of the (111) surface of a NaCl crystal created from an octopolar $(\text{NaCl})_4$ basis where the small circles represent the positive Na ions and the large ones the negative Cl ions. For the Cl ion terminated surface shown, micropyramids (consisting of three-ion Na clusters with a Cl ion residing above each cluster) are spaced in a $p(2 \times 2)$ pattern atop a close-packed layer of Cl ions.

uum (UHV) system operating at a base pressure of 5×10^{-11} mbar. LEED measurements were performed with a standard four-grid rear-view system. Details of the scanning tunneling microscope (STM) design have been described in an earlier publication.¹⁵ The UHV chamber also housed a quadrupole mass spectrometer for residual gas analysis and a hemispherical analyzer with an electron gun and ion gun for Auger electron spectroscopy and ion scattering spectroscopy measurements, respectively. The Au(111) sample was mounted on a tantalum plate and could be transferred between the sample manipulator and the STM with a wobble stick. Sample heating was performed either by radiative heating or electron bombardment from a tungsten filament mounted on the sample manipulator. Temperature measurement was performed with an optical pyrometer. Preparation of the Au(111) sample was performed by cycles of argon-ion bombardment ($E = 700$ eV) for $t \geq 45$ min followed by annealing to $T \sim 650^\circ\text{C}$ for ~ 20 min. Sample cleanliness was established by comparing the LEED and STM images of the Au(111) surface with previously published results. STM images of the clean surface clearly resolved the long-range $22 \times \sqrt{3}$ "herringbone" reconstruction which is characteristic of this surface,¹⁶ and, under ideal tunneling conditions, the atomic structure could also be resolved.

Ni deposition was performed with a Knudsen-type effusion cell equipped with a shutter to control the total amount of Ni deposited. During operation of the effusion cell, the pressure rise in the chamber was no greater than 2×10^{-10} mbar. The Ni deposition rate was monitored by a quartz crystal microbalance (QCM). For submonolayer coverages of Ni on Au(111), the Ni forms quasihexagonal two-dimensional islands which nucleate at the kinks of the Au(111) "herringbone" reconstruction.¹⁷ Therefore, a second confirmation of the Ni deposition rate was performed with the STM by measuring the relative surface area of the Ni islands to that of the Au substrate. NiO growth was performed by evaporating Ni at a rate of ~ 0.7 ML/min (Ref. 18) (where ML represents monolayers) in an oxygen atmosphere of 2×10^{-6} mbar onto a clean Au(111) crystal. The Ni evaporation rate was carefully monitored with the QCM to assure a stable evaporation rate to within $\sim 5\%$ before backfilling the chamber with oxygen and growing the NiO films.

For NiO growth on a Au(111) sample held at room temperature, both LEED and STM results revealed the growth of a three-domain NiO(100) crystallite structure with an average crystallite diameter of ~ 50 Å. These results contradict those of a recent combined LEED and ultraviolet photoelectron spectroscopy study of NiO growth on Au(111) by Ni deposition in an oxygen atmosphere where the growth of an unreconstructed NiO(111) structure was reported.¹⁹ Since pressure rises on the order of 10^{-8} mbar were recorded during operation of the Ni effusion cell used in that study, it is suspected that this surface has been stabilized by surface contaminants. Annealing the three-domain NiO(100) overlayer to $T \sim 300^\circ\text{C}$ revealed a dramatic reduction in the defect density of the NiO but left it in its three-domain NiO(100) crystalline form. At $T \sim 550^\circ\text{C}$, faceting of the

overlayer begins. Further details of the growth morphology of NiO on Au(111) at room temperature will be published in a future publication.²⁰

Since annealing the three-domain NiO(100) structure was found to increase the surface mobility of the NiO enough to heal defects, NiO growth on a Au sample held at $T \sim 300^\circ\text{C}$ was attempted to determine the possibility of growing a stable NiO(111) overlayer. Since Ni is slightly soluble in Au at this temperature (~ 7 at. %),²¹ Ni deposition on the clean Au(111) surface *without* oxygen was first attempted. STM images of submonolayer depositions of Ni resolved only the atomic structure of the clean Au(111) without Ni islands which is consistent with Ni solvation. However, for Ni deposition in an oxygen atmosphere onto a Au(111) sample held at $T \sim 300^\circ\text{C}$, the growth of $p(2 \times 2)$ reconstructed NiO(111) was resolved as seen by the LEED images shown in Fig. 2. The LEED image of the clean Au(111) surface at $E = 127$ eV, in Fig. 2(a), shows the hexagonal electron diffraction pattern which is expected for the (111) surface of an fcc lattice. Some additional streaking is also observed between the diffraction spots due to the long-range "herringbone" reconstruction of this surface.

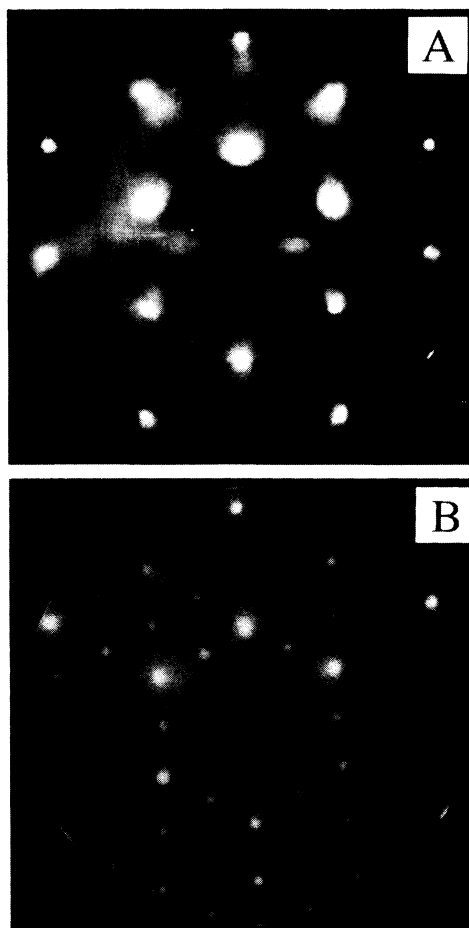


FIG. 2. LEED patterns at an electron energy of $E = 127$ eV of (a) the clean Au(111) surface, (b) the $p(2 \times 2)$ reconstructed NiO(111) grown by deposition of ~ 3 ML of Ni in an oxygen atmosphere of $\sim 2 \times 10^{-6}$ mbar onto a Au(111) crystal held at $T = 300^\circ\text{C}$.

The LEED image at $E = 127$ eV, which results when ~ 3 ML of Ni is deposited in an oxygen atmosphere onto Au(111) held at $T \sim 300^\circ\text{C}$, is shown in Fig. 2(b). This image reveals the same hexagonal diffraction pattern with an additional diffraction spot located between each primary spot which is indicative of a $p(2 \times 2)$ overlayer structure. This $p(2 \times 2)$ growth mode was stable up to ~ 6 ML of deposited Ni. Beyond this coverage, the LEED images indicated that a faceted structure exists.

To determine the atomic structure of the $p(2 \times 2)$ reconstructed overlayer which was resolved by LEED, STM images of this overlayer were measured. A $250 \times 250 \text{ \AA}^2$ constant tunneling current STM image of the $p(2 \times 2)$ reconstructed overlayer is shown in Fig. 3. Atomically resolved $p(2 \times 2)$ reconstructed regions and relatively flat (corrugation $< 0.2 \text{ \AA}$) regions where no atomic features are resolved can be seen in this image. Several missing-atom point defects also exist in the $p(2 \times 2)$ reconstructed region. The measured height difference between the flat regions and the top of the $p(2 \times 2)$ regions is $\sim 0.6 \text{ \AA}$ (flat regions higher). A step edge along the right side of the image is also resolved. The measured step height between the $p(2 \times 2)$ reconstructed terraces is $\sim 2.4 \text{ \AA}$ which indicates that the two terraces are terminated by the same ion. A $35 \times 50 \text{-\AA}^2$ STM image of the $p(2 \times 2)$ reconstructed surface is shown in Fig. 4(a). This image again shows atomically resolved $p(2 \times 2)$ reconstructed regions with several random missing-atom point defects. In this figure a tripod-like ridge structure is seen to emanate under each atomic protrusion. For negative sample bias, atomic resolution images were obtained over the range -5 to -0.3 V. However, for positive sample bias, atomic resolution images were only obtained at ~ 5 V. The measured corrugation height of the $p(2 \times 2)$ reconstructed regions and the relative height of the flat regions to that of the $p(2 \times 2)$ regions did not vary appreciably at any bias.

Occasionally the height of the flat regions of the sur-



FIG. 3. A $250 \times 250 \text{-\AA}^2$ STM image of the $p(2 \times 2)$ NiO(111) surface ($V_s = -5$ V, $I = 0.5$ nA). $p(2 \times 2)$ reconstructed regions with several missing-atom point defects, relatively flat regions (corrugation $< 0.2 \text{ \AA}$), and a step edge along the right side are resolved in this image. The measured height difference between the flat regions and the top of the $p(2 \times 2)$ regions is $\sim 0.6 \text{ \AA}$ (flat region higher).

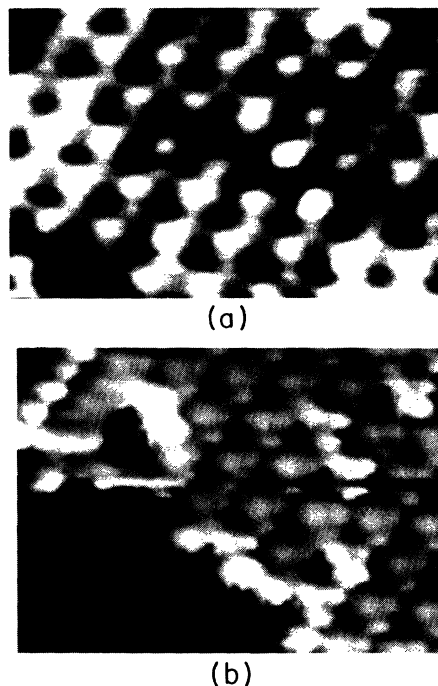


FIG. 4. High-resolution $35 \times 50 \text{-\AA}^2$ STM images of (a) the $p(2 \times 2)$ NiO(111) resolved with a metallic tip apex where a tripodlike ridge structure is seen to emanate under each atomic protrusion ($V_s = -5$ V, $I = 0.5$ nA), (b) the $p(2 \times 2)$ NiO(111) resolved with a nonmetallic tip apex where three-atom clusters are resolved on the $p(2 \times 2)$ regions ($V_s = -0.3$ V, $I = 0.5$ nA). An array of close-packed atoms with the same periodicity as the Au(111) surface is resolved in the lower-left regions. The measured height difference between the top of the $p(2 \times 2)$ region and the close-packed region is $\sim 0.7 \text{ \AA}$ [$p(2 \times 2)$ region higher].

face was seen to switch in a scan from residing $\sim 0.6 \text{ \AA}$ above the $p(2 \times 2)$ regions to residing $\sim 0.7 \text{ \AA}$ below them. A $35 \times 50 \text{-\AA}^2$ STM image for the later condition is shown in Fig. 4(b). Two striking changes in the topography are observed for this condition: atomic corrugations with a close-packed structure and lattice constant similar to the Au(111) surface are observed for the regions which were previously resolved as flat regions and three-atom clusters are observed where the micropylamidal structures of the $p(2 \times 2)$ regions were previously resolved. Scanning tunneling spectroscopy measurements performed above the flat regions for both situations has revealed that for the former situation, flat region above $p(2 \times 2)$, the measurement yields an Ohmic response from which we conclude that the tip apex is metallic tungsten. For the later condition, a response indicating the existence of a band gap is measured above the flat regions from which we conclude that the electronic property of the apex of the tip has changed to nonmetallic. The most probable origin of this change is the adsorption of a single oxygen atom at the tip apex during a scan.

Since a change in the electronic properties of the tip apex results in a dramatically different resolved structure within the unit cells of the oxide region, one cannot *a priori* differentiate which kind of atom is being imaged for a given tip apex. Therefore, the results of a recent STM

publication by Ruan *et al.*²² for the systems oxygen adsorbed on Ni(110) and oxygen adsorbed on Cu(110) have been used for the interpretation of our STM data. They concluded that for a metallic tungsten tip apex, only the oxygen atoms of the Ni(Cu)-O surface chains were resolved as protrusions. When an oxygen atom was controllably adsorbed at the apex of their tip, only the metal atoms were resolved as protrusions. Using this convention, the three-atom clusters observed in Fig. 4(b) should correspond to Ni ions, and the point of each micropyramid in Fig. 4(a) should correspond to a single oxygen atom. The measured step height of 2.4 Å between terraces of $p(2 \times 2)$ regions for all measured step edges also indicates that the $p(2 \times 2)$ regions are always terminated with the same ion. Since the theoretically predicted octopolar surface termination would consist of a series of three-ion clusters with an ion of opposite charge located above each cluster to form micropyramids (see Fig. 1), our results are consistent with this model. However, since the mechanism for resolving different chemical species with different tip apexes is not well understood at this time, a better theoretical understanding of this effect is needed before one can conclusively say that the resolved corrugations correspond to the octopolar surface termination.

The LEED and STM results give strong evidence that a $p(2 \times 2)$ NiO(111) overlayer has been formed. However, several possible origins other than the existence of a $p(2 \times 2)$ reconstructed NiO(111) have been considered to explain the experimental results. For instance, a $p(2 \times 2)$ chemisorbed oxygen or Ni overlayer on the Au(111) were considered for the origin of the $p(2 \times 2)$ structure. Since neither oxygen doping on clean Au(111) at 300 °C without a Ni flux nor Ni deposition without oxygen resulted in $p(2 \times 2)$ overlayers, these possibilities were discounted. It is also possible that a $p(2 \times 2)$ reconstructed Au(111) was created. However, stable tunneling could be achieved on clean Au(111) down to ~ 1 mV yet only to -300 mV for the $p(2 \times 2)$ structure which indicates that the $p(2 \times 2)$ surface is a semiconducting oxide. It was

also noted that chemisorbed oxygen on Ni(111) initially adsorbs in a $p(2 \times 2)$ structure.²³ However, the lattice constant of NiO is 19% greater than that of Ni which would be easily detectable with both LEED and STM. Since the formation of Ni₂O₃ and NiO₂ single crystals under high oxygen partial pressures have been reported,²¹ the possibility that nonstoichiometric NiO was created was also considered. However, the results of our LEED and STM analyses are not consistent with the known crystalline structure of either Ni₂O₃ or NiO₂.

The nonpolar NiO(100) surface appears to be more stable for growth at room temperature. However, at $T \sim 300$ °C Ni is slightly soluble in Au which we believe creates a dynamic growth process by which the impinging oxygen acts to draw the Ni out of the Ni/Au surface alloy. Under these conditions, the formation of a reconstructed NiO(111) surface is preferred. Due to the limited rate at which the oxygen can diffuse through the growing NiO(111) overlayer, this process is only stable for the first few monolayers of $p(2 \times 2)$ NiO(111) growth. Growth beyond a few monolayers results in large-scale facet formation. The surface topography of the $p(2 \times 2)$ NiO(111) surface resolved by STM is consistent with the theoretically predicted octopolar reconstruction for (111) terminated NaCl structured materials.^{1,5} However, further structural measurements, such as a LEED-IV study, are needed to more precisely determine the internal structure of the $p(2 \times 2)$ overlayer and the degree of relaxation present at the surface.

We would like to thank Professor N. J. DiNardo and Professor E. L. Garfunkel for their comments and suggestions and Professor H.-J. Freund and his colleagues for informative discussions on the preparation of NiO on Ni single crystals. The financial assistance provided by the Deutsche Forschungsgemeinschaft (DFG) is greatly appreciated. One of us (C.A.V.) would also like to thank the Graduiertenkolleg Dynamische Prozesse an Festkörperoberflächen Ruhr-Universität Bochum for financial support.

*Present address: Physics Department, Rensselaer Polytechnic Institute, 110 8th Street, Troy, New York 12180.

†Present address: MPI für Molekular Physiologie, Rheinlanddamm 201, D-44 139 Dortmund, Germany.

¹R. Lacmann, *Colloq. Int. C. N. R. S.* **152**, 195 (1965).

²R. W. Nosker and P. Mark, *Surf. Sci.* **19**, 291 (1970).

³M. Tsukada *et al.*, *J. Phys. Soc. Jpn.* **50**, 3032 (1981).

⁴P. A. Cox *et al.*, *Vacuum* **33**, 839 (1983).

⁵D. Wolf, *Phys. Rev. Lett.* **68**, 3315 (1992).

⁶N. Floquet and L.-C. DuFour, *Surf. Sci.* **126**, 543 (1983).

⁷P. A. Cox and A. A. Williams, *Surf. Sci.* **152/153**, 791 (1985).

⁸S. Andersson and J. W. Davenport, *Solid State Commun.* **28**, 677 (1978).

⁹S. Hüfner *et al.*, *Z. Phys. B* **83**, 185 (1991).

¹⁰V. E. Henrich, *Rep. Prog. Phys.* **48**, 1481 (1985).

¹¹H. Kühlenbeck *et al.*, *Phys. Rev. B* **43**, 1969 (1991).

¹²M. Bäumer *et al.*, *Surf. Sci.* **253**, 116 (1991).

¹³W. Weiss and G. A. Somorjai, *J. Vac. Sci. Technol. A* **11**, 2138 (1993).

¹⁴W. Weiss *et al.*, *Phys. Rev. Lett.* **71**, 1848 (1993); A. Barbieri *et al.*, *Surf. Sci.* (to be published).

¹⁵Th. Berghaus *et al.*, *Surf. Sci.* **184**, 273 (1987).

¹⁶Ch. Wöll *et al.*, *Phys. Rev. B* **39**, 7988 (1989).

¹⁷D. D. Chambliss *et al.*, *Phys. Rev. Lett.* **66**, 1721 (1991).

¹⁸We reference 1 ML to the number density of a close-packed Au(111) layer.

¹⁹K. Marre and H. Neddermeyer, *Surf. Sci.* **287/288**, 995 (1993).

²⁰H. Hannemann, Th. Bertrams, C. A. Ventrice, Jr., A. Brodde, and H. Neddermeyer (unpublished).

²¹Max Hansen, *Constitution of Binary Alloys*, 2nd ed. (McGraw-Hill, New York, 1958).

²²L. Ruan *et al.*, *Phys. Rev. Lett.* **70**, 4079 (1993).

²³A. R. Kortan and R. L. Park, *Phys. Rev. B* **23**, 6340 (1981).

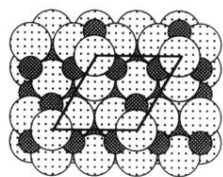


FIG. 1. Schematic of the top view of the (111) surface of a NaCl crystal created from an octopolar $(\text{NaCl})_4$ basis where the small circles represent the positive Na ions and the large ones the negative Cl ions. For the Cl ion terminated surface shown, micropyramids (consisting of three-ion Na clusters with a Cl ion residing above each cluster) are spaced in a $p(2 \times 2)$ pattern atop a close-packed layer of Cl ions.

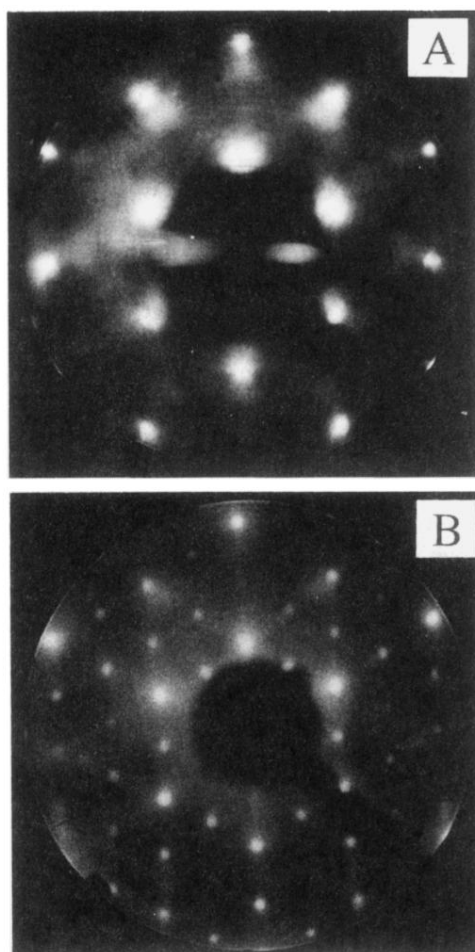


FIG. 2. LEED patterns at an electron energy of $E = 127$ eV of (a) the clean Au(111) surface, (b) the $p(2 \times 2)$ reconstructed NiO(111) grown by deposition of ~ 3 ML of Ni in an oxygen atmosphere of $\sim 2 \times 10^{-6}$ mbar onto a Au(111) crystal held at $T = 300^\circ\text{C}$.

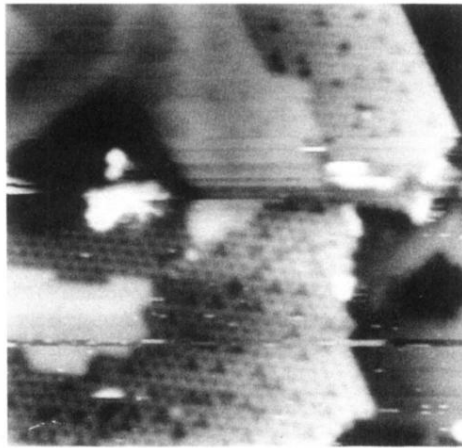
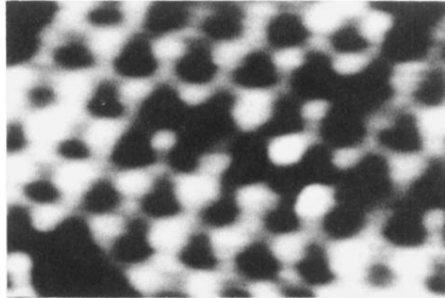
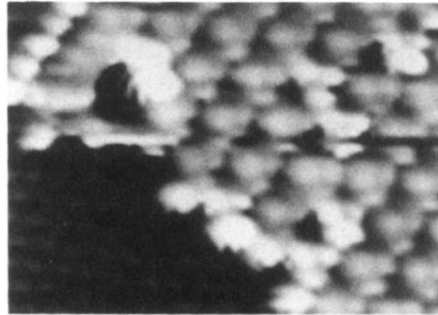


FIG. 3. A $250 \times 250\text{-\AA}^2$ STM image of the $p(2 \times 2)$ NiO(111) surface ($V_s = -5\text{ V}$, $I = 0.5\text{ nA}$). $p(2 \times 2)$ reconstructed regions with several missing-atom point defects, relatively flat regions (corrugation $< 0.2\text{ \AA}$), and a step edge along the right side are resolved in this image. The measured height difference between the flat regions and the top of the $p(2 \times 2)$ regions is $\sim 0.6\text{ \AA}$ (flat region higher).



(a)



(b)

FIG. 4. High-resolution $35 \times 50\text{-}\text{\AA}^2$ STM images of (a) the $p(2 \times 2)$ NiO(111) resolved with a metallic tip apex where a tripodlike ridge structure is seen to emanate under each atomic protrusion ($V_s = -5$ V, $I = 0.5$ nA), (b) the $p(2 \times 2)$ NiO(111) resolved with a nonmetallic tip apex where three-atom clusters are resolved on the $p(2 \times 2)$ regions ($V_s = -0.3$ V, $I = 0.5$ nA). An array of close-packed atoms with the same periodicity as the Au(111) surface is resolved in the lower-left regions. The measured height difference between the top of the $p(2 \times 2)$ region and the close-packed region is ~ 0.7 \AA [$p(2 \times 2)$ region higher].